

PAPER • OPEN ACCESS

Probing the interaction between 2D materials and oligoglycine tectomers

To cite this article: Manoj Tripathi *et al* 2022 *2D Mater.* **9** 045033

View the [article online](#) for updates and enhancements.

You may also like

- [A strategic review of recent progress, prospects and challenges of MoS₂-based photodetectors](#)
Riya Wadhwa, Abhay V Agrawal and Mukesh Kumar
- [Lysozyme-assisted ultrasonic exfoliation of graphitic carbon nitride into highly stable nanosheets with enhanced bactericidal capacity](#)
Liang-Liang Chen, Wen-Pu Shi, Tuo-Di Zhang et al.
- [Recent progress in two dimensional Mxenes for photocatalysis: a critical review](#)
Tahir Haneef, Kashif Rasool, Jibran Iqbal et al.



PAPER

OPEN ACCESS

RECEIVED
25 July 2022

REVISED
9 September 2022

ACCEPTED FOR PUBLICATION
18 September 2022

PUBLISHED
5 October 2022

Original content from
this work may be used
under the terms of the
[Creative Commons
Attribution 4.0 licence](#).

Any further distribution
of this work must
maintain attribution to
the author(s) and the title
of the work, journal
citation and DOI.



Probing the interaction between 2D materials and oligoglycine tectomers

Manoj Tripathi^{1,*} , Rosa Garriga^{2,*} , Frank Lee¹ , Sean P Ogilvie¹ , Aline Amorim Graf¹ ,
Matthew J Large¹ , Peter J Lynch¹ , Konstantinos Papagelis³ , John Parthenios⁴ ,
Vicente L Cebolla⁵ , Izabela Jurewicz^{6,7} , Alan B Dalton^{1,*} and Edgar Muñoz⁵

¹ Department of Physics and Astronomy, University of Sussex, Brighton BN1 9RH, United Kingdom

² Departamento de Química Física, Universidad de Zaragoza, Pedro Cerbuna, 12, 50009 Zaragoza, Spain

³ School of Physics, Department of Solid-State Physics, Aristotle University of Thessaloniki, Thessaloniki 54124, Greece

⁴ Institute of Chemical Engineering Sciences, Foundation for Research and Technology-Hellas (FORTH/ICE-HT), Patras 26504, Greece

⁵ Instituto de Carboquímica ICB-CSIC, Miguel Luesma Castán 4, 50018 Zaragoza, Spain

⁶ Department of Physics, Faculty of Engineering and Physical Sciences, University of Surrey, Guildford GU2 7XH, United Kingdom

⁷ Advanced Material Development Ltd, Surrey Technology Centre, 40 Occam Rd, Guildford GU2 7YG, United Kingdom

* Authors to whom any correspondence should be addressed.

E-mail: m.tripathi@sussex.ac.uk, rosa@unizar.es and A.B.Dalton@sussex.ac.uk

Keywords: heterostructure, 2D materials, peptide assemblies, adhesion force, strain, doping, Raman spectroscopy

Supplementary material for this article is available [online](#)

Abstract

Heterostructures of two-dimensional (2D) materials using graphene and MoS₂ have enabled both pivotal fundamental studies and unprecedented sensing properties. These heterosystems are intriguing when graphene and MoS₂ are interfaced with 2D sheets that emulate biomolecules, such as amino-terminated oligoglycine self-assemblies (known as tectomers). The adsorption of tectomer sheets over graphene and MoS₂ modulates the physicochemical properties through electronic charge migration and mechanical stress transfer. Here, we present a systematic study by Raman spectroscopy and tectomer-functionalised scanning probe microscopy to understand mechanical strain, charge transfer and binding affinity in tectomer/graphene and tectomer/MoS₂ hybrid structures. Raman mapping reveals distinctive thickness dependence of tectomer-induced charge transfer to MoS₂, showing p-doping on monolayer MoS₂ and n-doping on multilayer MoS₂. By contrast, graphene is n-doped by tectomer independently of layer number, as confirmed by x-ray photoelectron spectroscopy. The interfacial adhesion between the amino groups and 2D materials are further explored using tectomer-functionalised probe microscopy. It is demonstrated here that these probes have potential for chemically sensitive imaging of 2D materials, which will be useful for mapping chemically distinct domains of surfaces and the number of layers. The facile tectomer-coating approach described here is an attractive soft-chemistry strategy for high-density amine-functionalisation of atomic force microscopy probes, therefore opening promising avenues for sensor applications.

1. Introduction

There is significant research interest in exploring the modulation of mechanical and physicochemical properties when interfacing different two-dimensional (2D) materials. Such vertical heterostructures using graphene, transition metal dichalcogenides (such as MoS₂ and WS₂), and hexagonal boron nitride can exhibit electronic doping

and strain phenomena as well as other synergies such as moiré superlattice which can improve device performance in myriads of applications [1–10]. Beyond conventional 2D materials, coupling these nanosheets with derivatives of biomolecules such as peptides and their assemblies can modulate the intrinsic physical properties of 2D materials and provide new functionalities as well as processing versatility. Thus, it enables the use of these nanosheets as the platform

for chemical and biosensing applications in biomedicine, bioelectronics and micro-mechanical devices [11–16].

Most of these sensor applications are based on non-covalent interactions at the interface between 2D material-based sensing layers and the biomolecules of interest that preserve the electrical properties and intrinsic strength of the 2D materials [17], in contrast to defect-induced detection [18]. In graphene, sp^2 hybridised carbon atoms are arranged in a long-range π conjugation acting as a semi-metal. During the physisorption of foreign species, these conjugated systems recognise subtle changes in electronic and physical characteristics. While chalcogenides such as MoS_2 have a trilayer configuration of S–Mo–S, they demonstrate thickness-dependent electronic and optical properties. Monolayer MoS_2 is a semiconductor ($E_g \approx 1.9$ eV) and is extremely sensitive towards physisorbed foreign molecules at its basal plane through electrostatic and van der Waals interactions [19, 20]. One of the general mechanisms of sensing foreign entities attached to the 2D sheets is to measure the shifting of Fermi level as a result of the induced n- or p-doping [21]. Several studies have demonstrated the ability of graphene- and MoS_2 -based biosensors to detect DNA-protein complexes, nucleobases and amino acids [21–23].

The influence of the interactions with biomolecular species on graphene and MoS_2 sheets can be envisioned in terms of locally induced mechanical strain (π) and charge carrier density (n) compared to their pristine state. There are several detection techniques, namely fluorescence, colourimetry, electrochemiluminescence, etc, which have been implemented to detect the changes in the adsorbed system [24, 25]. Raman spectroscopic imaging is another powerful experimental technique to study these physicochemical interactions in graphene and MoS_2 , which has been established as a promising non-destructive tool to evaluate the mechanical strain and carrier density [26, 27]. The Raman modes G (E_{2g}^1) and 2D (A_{1g}) of graphene (MoS_2) are known to be associated with the change of interatomic distances and the redistribution of charge carriers [28–30]. The interactions of graphene and MoS_2 can also be visualised by measuring the interfacial adhesion, which is only indirectly probed by spectroscopic techniques [31], and thus, a direct alternative would be atomic force microscopy (AFM) with the state-of-the-art concept of probe functionalisation [32, 33].

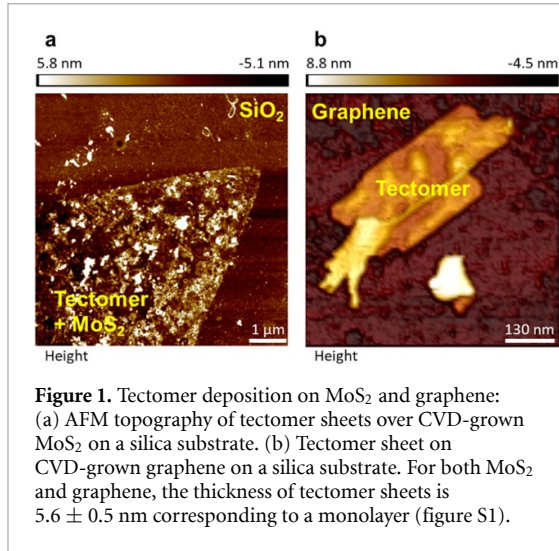
The complementary use of Raman mapping and scanning probing techniques is useful in gathering interfacial interaction between 2D materials and biomolecules such as oligopeptides. The advantage of using a peptide-based assembly to develop this sensing approach is that they emulate the diversity of a range of biological structures and functional groups such as DNA and

amino acids [34]. Amino-terminated oligoglycine peptides consist of antennae of typically four to seven glycine units connected by alkyl linkers, $C_8H_{16}(-CH_2-NH-Gly_4)_2$. These oligopeptides self-assemble into sheet-like 2D structures (single-layered platelet thickness ~ 5.6 nm) through cooperative hydrogen bonding between adjacent glycine units in neighbouring antennae. The oligoglycine assembly is pH-responsive, a unique feature among 2D materials, that allows the controlled load and release of cargo as a function of pH [34, 35]. Additionally, surface amino groups in the tectomer provide remarkable adhesive properties that can be exploited to coat and provide new functions to a range of substrates by efficiently attaching a variety of molecules and nanoparticles. Previous research suggests tectomers can exhibit ambipolar charge transfer, and thus the significant areal doping when successfully interfaced with other 2D nanomaterials can be utilised for the fabrication of novel layered composite materials [35, 36].

In the present work, we show that the binding affinities of the amine surface groups of tectomers with MoS_2 and graphene nanosheets lead to specific changes in charge carrier density and mechanical strain, which are monitored by Raman mapping. In addition, AFM probe functionalisation by wrapping tectomer around the tip apex provides spatially resolved information on interfacial interaction as well as quantitative measurement of critical adhesion force (pull-out) between tectomers and the 2D materials tested. Thus, it is demonstrated here that these probes have potential for chemically sensitive imaging of 2D materials, which will be useful for mapping chemically distinct domains of surfaces and the number of layers. The measured interfacial adhesion force values show a similar trend with binding energy (BE) shifts of N1s peaks in tectomers from x-ray photoelectron spectroscopy (XPS). The results reported here open attractive avenues for the use of amino-terminated oligopeptides in the development of future surface and chemical sensors as well as the fabrication of novel functional heterostructures with other 2D materials.

2. Results and discussion

AFM topography of tectomers deposited on MoS_2 and graphene on silica substrates are shown in figures 1(a) and (b) respectively. Chemical vapour deposition (CVD) grown MoS_2 is in the form of triangular monolayer island, while CVD grown graphene was transferred onto silica as a continuous single layer (1L) with bilayer (2L) islands. Over both surfaces, the thickness of the deposited tectomer sheets is 5.6 ± 0.5 nm, corresponding to a monolayer (see supplementary figure S1 for details) [34, 37]. The effect of tectomer deposition on mechanical strain and doping



in MoS₂ and graphene is then studied by Raman spectroscopic mapping.

The typical Raman spectra of bare 1L MoS₂ and tectomer-coated 1L MoS₂ are compared in figure 2(a). The Raman bands for bare 1L MoS₂ corresponding to the in-plane vibrations (E_{2g}^1) and out-of-plane vibrations (A_{1g}) of Mo and S atoms are located at approximately 385 cm^{-1} and 405 cm^{-1} respectively [27, 38], where the Raman peak difference ($A_{1g}\omega - E_{2g}^1\omega$) of $\sim 20 \text{ cm}^{-1}$ confirms that it is a monolayer [39]. Additional AFM images for the monolayer can be found in figure S2. Upon tectomer coating of MoS₂, the E_{2g}^1 mode downshifts while the A_{1g} mode upshifts. To study this effect extensively, Raman mapping of bare 1L MoS₂ (figures 2(b) and (c)) and tectomer-coated 1L MoS₂ (figures 2(d) and (e)) are carried out by collecting spectral data within the same region, which can be used to extract strain (ε) and charge carrier density (n) in MoS₂ by a generalised linear transformation (equation (1)):

$$\begin{pmatrix} \omega_1 \\ \omega_2 \end{pmatrix} = \begin{pmatrix} -2\gamma_1\omega_1^0 & k_1 \\ -2\gamma_2\omega_2^0 & k_2 \end{pmatrix} \begin{pmatrix} \varepsilon \\ n \end{pmatrix} \quad (1)$$

where γ is the Grüneisen parameter, k is the doping sensitivity, and ω^0 is the absence of strain and doping frequency. The subscript 1 and 2 represents E_{2g}^1 and A_{1g} mode where constant values are respectively $\gamma_{E_{2g}^1} = 0.86$, $\gamma_{A_{1g}} = 0.15$, $k_{E_{2g}^1} = -0.33 \times 10^{-13} \text{ cm}^{-1}$, and $k_{A_{1g}} = -2.22 \times 10^{-13} \text{ cm}^{-1}$ [30, 40]. Using equation (1), a correlation plot of $A_{1g}\omega$ against $E_{2g}^1\omega$ (figure 2(f)) can be plotted with contour lines (marked as grey dashed lines) representing equal level of strain and carrier concentration. The point of intersection of the strain axis (in pink) and the doping axis (in brown) calculated as $(384.9 \pm 0.4 \text{ cm}^{-1}, 405.0 \pm 0.2 \text{ cm}^{-1})$ provides the average value of strain and doping of bare MoS₂. The distribution and the histogram of the data is illustrated in figure S3. Thus, the deviation

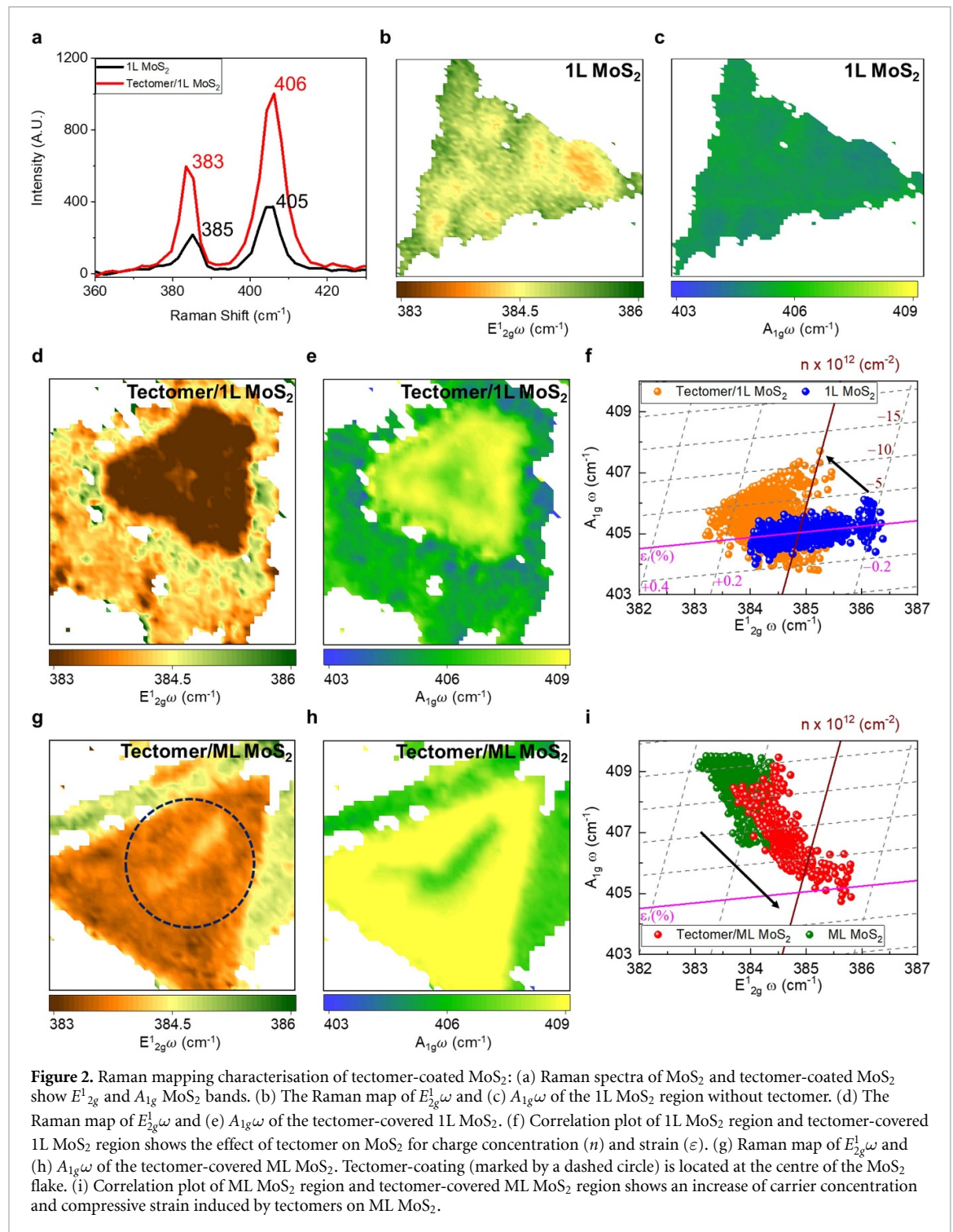
from the intersection in the Raman modes represents the locally induced strain and doping due to the interaction with tectomer.

These results show that tectomer coating modifies the Raman shifts of E_{2g}^1 and A_{1g} mode in 1L MoS₂ to $(384.2 \pm 0.3) \text{ cm}^{-1}$ and $(405.8 \pm 0.4) \text{ cm}^{-1}$ respectively, indicating a surface morphology change by mechanical stretching which induces a tensile strain increase of $(0.11 \pm 0.05) \%$, as well as a decrease in charge carrier density by $(4.0 \pm 1.8) \times 10^{12} \text{ cm}^{-2}$ (as indicated by the black arrow in figure 2(f)), i.e. p-doping to 1L MoS₂. The distribution of the above data can be found in the histogram in figure S3. On the other hand, the correlation plot used for multilayer (ML) MoS₂-tectomer system (figures 2(g)–(i)) is limited to a qualitative description as the layer number itself will have an influence on the peak positions (see figure S2 for the thickness distribution and Raman mapping of ML MoS₂). Nevertheless, the shift of the Raman modes of ML MoS₂ indicates n-doping and compressive strain induced by tectomer (black arrow in figure 2(i)). This clearly illustrates that the changes in MoS₂ carrier concentration imposed by tectomer decoration are layer dependent.

As for graphene, the tectomer coating induces downshift of 6 cm^{-1} and 2 cm^{-1} of the G and 2D Raman modes respectively as illustrated in the typical Raman spectra (figure 3(a)), where the additional peak at 1654 cm^{-1} shows the presence of polyglycine II type crystalline structure that results from the oligoglycine self-assembly [41]. The effect of tectomer coating on modulating strain and doping in 1L graphene (see figure S2 for the thickness measurement by AFM) can also be calculated by the linear transformation in equation (1), where the subscript 1 and 2 are now replaced by G and 2D modes and the corresponding constants are $\gamma_G = 1.95$, $\gamma_{2D} = 3.15$, $k_G = -1.407 \times 10^{-12} \text{ cm}^{-1}$ and $k_{2D} = -0.285 \times 10^{-12} \text{ cm}^{-1}$ [26, 42]. The resulting correlation plot in figure 3(b) shows the increase in electron concentration (less p-doping) of $(4.9 \pm 1.6) \times 10^{12} \text{ cm}^{-2}$ in graphene induced by the tectomer decoration (see figure S3 for the distribution of data). Nevertheless, the strain in graphene layer does not alter significantly when interfaced with tectomer, and the whole system remains in compressive strain, which is typical for the graphene/silica interface [43]. Given the minimal strain exerted on 1L graphene upon tectomer coating, G_ω linearly varies with the absolute value of the Fermi level from the Dirac point $|E_F|$ (equation (2)) [44, 45]:

$$G_\omega - 1580 = |E_F| \times 42 \text{ cm}^{-1} \text{ eV}^{-1}. \quad (2)$$

A significant shift in E_F of $(290 \pm 90) \text{ meV}$ can be calculated for graphene with adsorbed tectomer. These results reveal that tectomer sheets modify the electronic carrier concentration of 1L graphene



(and, therefore, act as dopants) but do not induce mechanical strain. Also, 2L graphene has shown a similar response as its 1L counterpart (figure 3(c)), i.e. tectomer leads to an increase in carrier concentration (n -doping) in graphene without significant modulation of strain as indicated by the redshift in G and 2D peak positions.

XPS characterisation reveals the interactions established by the amino groups on the tectomer surface with MoS₂ or graphene by monitoring the changes in N1s XPS spectra of tectomer/ML MoS₂

and tectomer/ML graphene. The identification of the N1s peak requires a comprehensive analysis of the spectra near the Mo3p_{3/2} peak centred at 395.2 eV as it overlaps the N1s region. In figure 4(a), the peak at 399.6 eV corresponds to the nitrogen atoms in the oligoglycine antennae of tectomers. The 2.0 eV shift towards higher BE in the presence of MoS₂ (figures 4(a) and (c)) indicates the donation of electron density (n -doping) from tectomer amino surface groups towards ML MoS₂, which is consistent with Raman spectroscopy results. Figure

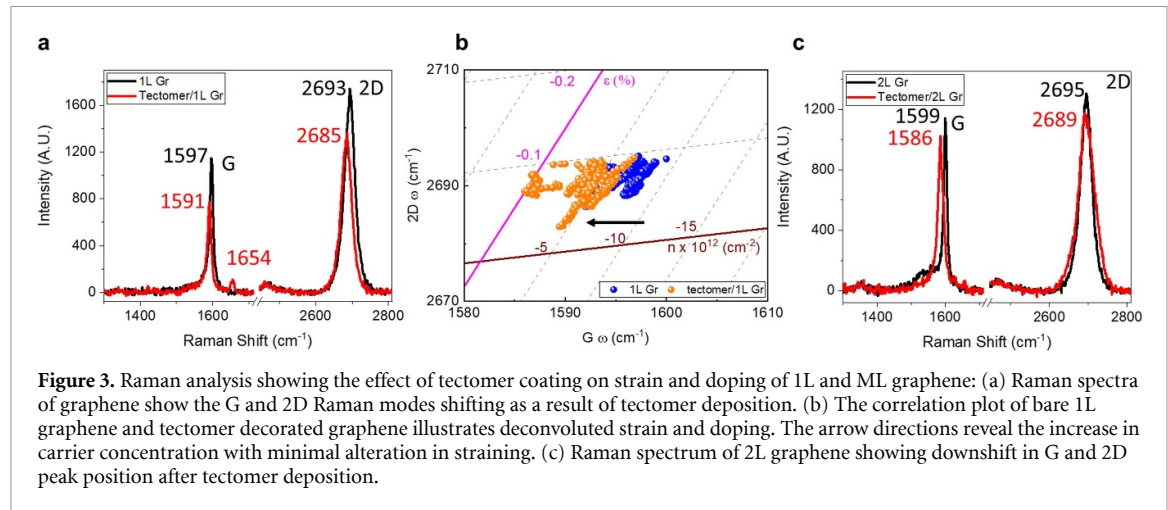


Figure 3. Raman analysis showing the effect of tectomer coating on strain and doping of 1L and ML graphene: (a) Raman spectra of graphene show the G and 2D Raman modes shifting as a result of tectomer deposition. (b) The correlation plot of bare 1L graphene and tectomer decorated graphene illustrates deconvoluted strain and doping. The arrow directions reveal the increase in carrier concentration with minimal alteration in straining. (c) Raman spectrum of 2L graphene showing downshift in G and 2D peak position after tectomer deposition.

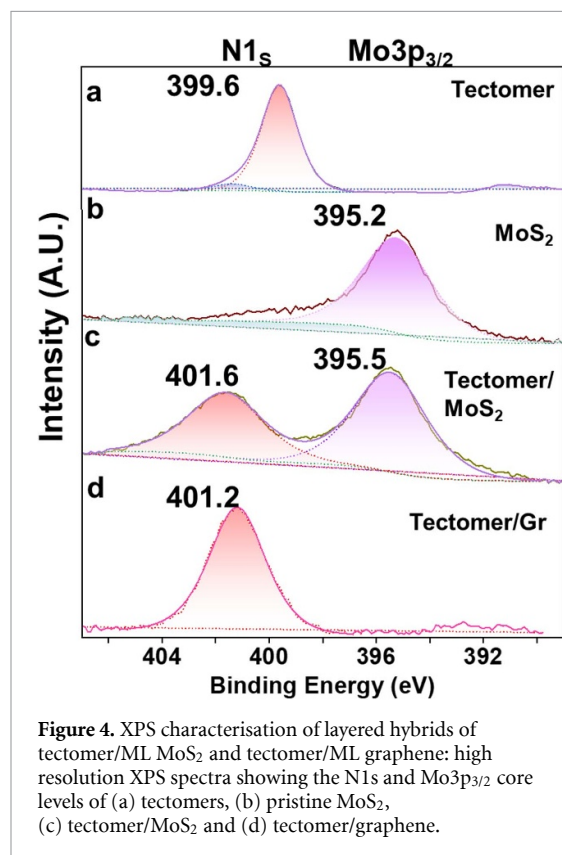


Figure 4. XPS characterisation of layered hybrids of tectomer/ML MoS₂ and tectomer/ML graphene: high resolution XPS spectra showing the N1s and Mo3p_{3/2} core levels of (a) tectomers, (b) pristine MoS₂, (c) tectomer/MoS₂ and (d) tectomer/graphene.

S3 shows S2p and Mo3d XPS spectra of pristine MoS₂ and tectomer/MoS₂ hybrids. The two identified doublets are characteristic of the S²⁻ and Mo⁴⁺ features presented in pristine MoS₂ [46]. Interestingly, all peaks in the XPS spectra in figure S4 are shifted identically to higher BE ~ 0.3 eV in tectomer/MoS₂ hybrids with respect to pristine MoS₂, suggesting a change in the Fermi level associated with n-doping [47, 48]. On the other hand, for tectomer/ML graphene, N1s XPS spectra exhibit a 1.6 eV shift towards higher BE (figures 4(a) and (d)) that can be explained by charge transfer (n-type doping) of amino groups in tectomers into

the π -system in graphene. Also, a shift of 1.6 eV in N1s XPS spectra was previously measured for other graphene-based material, such as carbon nanotubes, where the donation of electrons from amino groups in tectomers to the π -system of carbon nanotubes also occurs [36]. Further characterisation of tectomer/MoS₂ and tectomer/graphene hybrids by transmission electron microscopy (TEM), scanning electron microscopy (SEM) and energy dispersive X-ray (EDX) analysis are shown in figures S5 and S6. The effect of electrical doping from tectomer to ML MoS₂ and ML graphene can also be validated by I - V characterisation as a function of different bias voltages (-2 to 2 V), and at constant applied voltage (1 V) as a function of time (s). A sharp distinction in the resistance trend has been observed for graphene (increasing) and MoS₂ (decreasing). Given graphene usually being p-type and MoS₂ being n-type, this suggests tectomer n-dope both ML graphene and ML MoS₂. These results corroborated Raman spectroscopy and XPS results which suggest n-doping of tectomer to both ML graphene and MoS₂ (see supplementary information figure S7 for details).

Raman spectroscopy and XPS results indicate that tectomers interact differently with MoS₂ and graphene, leading to specific changes in charge carrier density, mechanical strain, and BE. This distinctive tectomer interaction towards 2D materials could be exploited in the development of tectomer-based surface recognition sensors. As a proof-of-concept, the interfacial interaction of tectomers with MoS₂ and graphene was characterised using tectomer-functionalised AFM probes, so routine adhesion force AFM measurements through force-distance spectroscopy provide the specified interfacial interaction between the surface amino terminated groups of tectomers and the scanned samples [33, 49]. Figure 5(a) illustrates a pristine AFM tip with a radius of 70 nm, which increases to 250 nm upon tectomer coating (figures 5(b) and (c)). The schematic representation

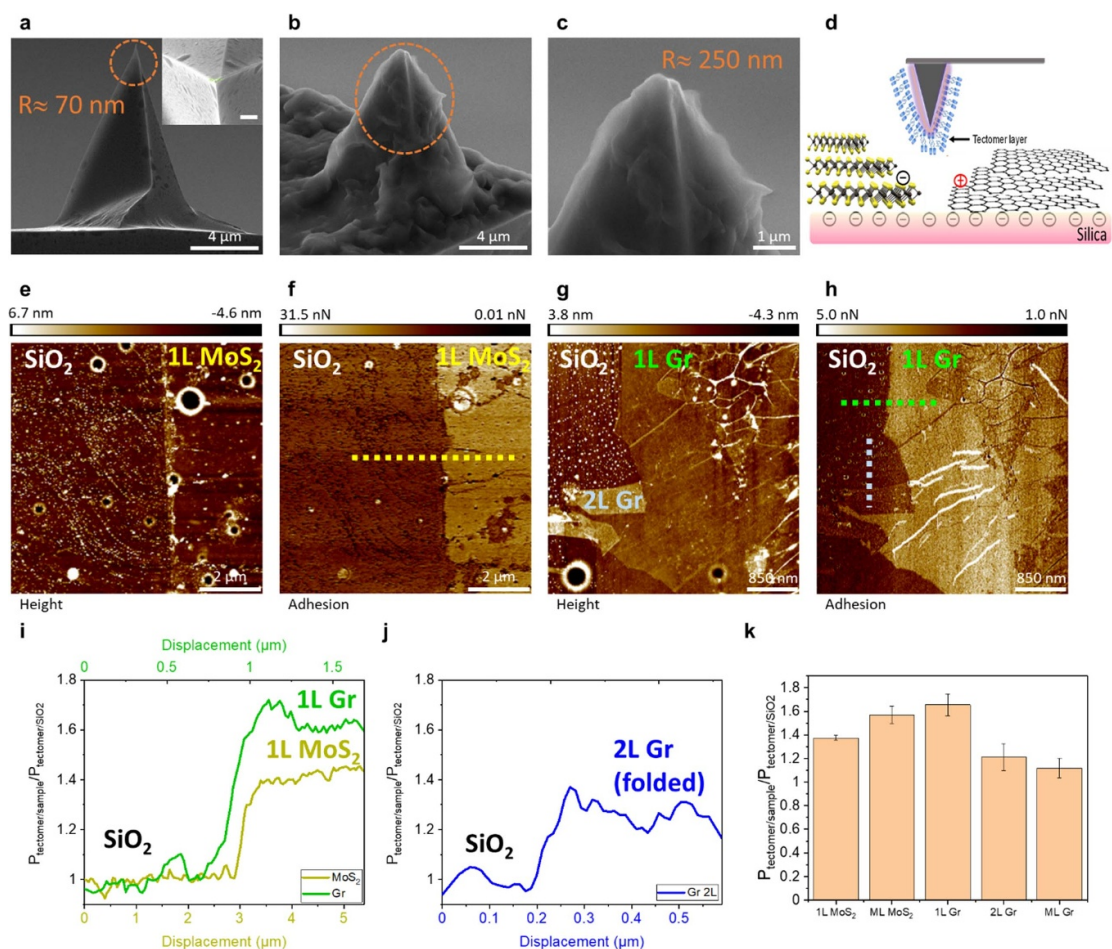


Figure 5. Interaction between tectomer-functionalised AFM probes and 2D materials: (a) SEM image of pristine AFM tip. Inset shows the encircled tip apex in high resolution, revealing a radius of 70 nm. (b) SEM image of tectomer-coated AFM tip apex and (c) the zoomed image shows the radius increases to 250 nm. (d) Schematic diagram of tectomer-coated AFM tip scanning on MoS₂ and graphene (Gr). (e), (f) AFM morphology and adhesion force map of the tectomer-coated tip scanning over silica-MoS₂ and (g), (h) silica-graphene. (i), (j) Adhesive pressure ratio profile of silica-MoS₂, silica-graphene and graphene wrinkle. (k) The distribution of adhesive pressure ratio varies over different surfaces showing that the tectomer-coated AFM probe is sensitive to the number of layers.

of functionalised probe microscopy over graphene and MoS₂ is shown in figure 5(d). The interaction between bare Pt/Ir-coated Si probe apex towards tectomer sheets as a function of time, AFM images showing minimal adhesion affinity dependence on tectomer thickness, and a separate study on the mass of the tectomer deposited over the cantilever are included in supplementary information figures S8–S10, respectively.

Adhesion force measurements are performed using tectomer-functionalised AFM probes scanning over 1L MoS₂ and 1L graphene deposited on silica substrates as illustrated in figures 5(e), (f) and (g), (h) respectively. There is a significant contrast in the adhesion force maps measured for silica substrate, graphene and MoS₂ layers. The conversion of absolute adhesion force values into adhesive pressure [33] is attained by normalizing the adhesion force values from silica substrate at the same acquisition and introducing the adhesive pressure ratio between tectomer/2D materials and tectomer/silica.

This normalisation provides measurements independent of the contact area between tip apex and the surface. The adhesive pressure values of tectomer-functionalised tip towards 1L graphene being nearly 25% higher than 1L MoS₂ (figure 5(i)) reveals its chemical selectivity towards surface carbon and sulphur atoms. Moreover, the tectomer-functionalised probe is sensitive to the number of layers for both graphene and MoS₂ and shows a clear distinction in adhesion force values with different layer(s) in the following order: 1L graphene > ML MoS₂ > 1L MoS₂ > 2L (folded) graphene > ML graphene (figures 5(j) and (k)). While the adhesion of tectomer/1L graphene is higher than that tectomer/1L MoS₂, the adhesion of graphene (MoS₂) decreases (increases) with layer number and eventually the adhesion of tectomer/ML graphene becomes lower than that of tectomer/ML MoS₂.

The overall distribution of the adhesive pressure values could be explained using the reference from XPS results. The higher BE shift of tectomer/ML

MoS₂ than tectomer/ML graphene reveals stronger interaction of tectomer towards ML MoS₂. However, graphene/silica and MoS₂/silica system offer different layer-dependent electrostatic interaction due to variations in the densities of carrier types (i.e. p-type and n-type). The concentration of their respective charge carriers depends on the number of layers due to screening effect [50, 51]. Graphene is usually a p-doped system on silica substrate [43, 52]. Thus, 1L graphene is rich in hole carriers which gradually decrease with increasing the number of layers [50]. Given that amino-terminated tectomers are susceptible to donating electrons, the interfacial adhesion will be stronger for a more positively charged surface (such as 1L graphene/silica), than a less positively charged surface (2L graphene/silica). In contrast, the three-layered structure (S–Mo–S) in MoS₂ has a different interaction with silica substrate (typically n-doped) [52, 53]. With increasing the number of MoS₂ layers, charge screening together with the effect of adsorbed airborne impurities (charge trapping centres, e.g. water molecules) [51] lead to less n-doping (more positive charges). Consequently, electron density donation from tectomer and hence the interfacial adhesion will be stronger for thicker MoS₂.

It is worth noting that the AFM-based elastic indentation depth is lower for the MLs for both graphene and MoS₂ (figure S11), and thus lower contact area between the functionalised probe apex and the 2D materials is expected. Therefore, the interaction between the functionalised probe and graphene or MoS₂ will be primarily influenced by the charge distribution at the surface rather than mechanical indentation. The trend of adhesion force values can be validated through a separate experiment (figure S12) where silicon wafer (covered with native oxide) is stimulated at different bias voltages (−2, 0, 2 V) to monitor the electrostatic adhesion towards tectomer coated probe. It has been observed that negative bias voltage results in lower adhesion force value, which is gradually increasing with the positive bias. Thus, interfacial interaction between the amino-terminated functionalised probe with its counter surfaces is dominated by localised charge domains over the substrate.

3. Conclusion

A 2D material-based sensing is demonstrated using graphene and MoS₂ against amino-terminated oligoglycine. The versatile surface chemistry provided by the surface amino groups of tectomers enables the fabrication of novel heterostructures with other 2D nanomaterials, inducing changes in the mechanical strain and carrier density of the (semi)conducting materials. Functionalised probe microscopy in conjunction with Raman mapping and XPS reveals valuable insights into interfacial interactions. The different susceptibilities of tectomer to modulate the

properties of 1L and ML MoS₂ is discussed towards strain and doping; p-doping and tension is observed for 1L MoS₂ and n-doping and compression for ML MoS₂. In contrast, graphene is always n-doped by the amine groups of tectomer sheet independently of the layer number. Interestingly, no additional strain has been observed in both 1L and 2L graphene from the tectomers which is useful to monitor the modulation of the Fermi level. It is also demonstrated that tectomer-functionalised AFM probes present the possibility of chemically sensitive imaging of 2D materials which will be useful for mapping chemically distinct domains of surfaces. The facile tectomer-coating approach described here is an attractive soft-chemistry strategy for high-density amine-functionalisation of AFM probes. These amine groups allow further functionalisation for molecular recognition imaging, therefore opening promising avenues for sensor applications.

4. Materials and methods

4.1. Preparation of MoS₂ and graphene

The fabrication of MoS₂ crystals island over silica is comprehensively described in the literature [54]. A silicon wafer with a 90 nm silica oxide layer is spin coated by aqueous solution of NaMoO₄ (concentration 2 mg ml^{−1}). The coated wafer is placed in the furnace equipped with two different temperature settings, i.e. 750 °C with a rate of 10 °C min^{−1} and 230 °C. During the second stage of temperature treatment, the quartz crucible loaded with S (2 g) and treated for 15 min at the same temperature. Later the sample is removed from the furnace and allowed to cool at room temperature.

Single layer CVD graphene over silica was purchased from Graphenea (Graphenea, Inc. Spain). The distribution of 1L graphene was monitored through Raman mapping. Mechanically exfoliated graphene was fabricated through scotch tape method and deposited over 90 nm thick silica.

4.2. Preparation of tectomer

Biantennary oligoglycine peptide (C₈H₁₆(−CH₂−NH−Gly₄)₂ × 2HCl, purity >95%) was supplied by PlasmaChem GmbH. Tectomers resulted from the self-assembly of oligoglycine solutions in ultrapure water (Siemens LaboStar DI/UV 2 system, resistivity: 18.2 MΩ cm at 25 °C) bath sonicated (100 W Branson 2510 bath sonicator) for 3 min.

4.3. Preparation of tectomer/MoS₂ and tectomer/graphene hybrids for XPS characterisation

Liquid-phase exfoliated MoS₂ dispersion in cyclopentanone (CPO) (0.45 mg ml^{−1}) was prepared by a procedure that involves successive sonication of MoS₂ powder samples and centrifugation steps. Tectomers are poorly soluble in CPO; thus, solubilisation

of tectomers in CPO and subsequent tectomer/MoS₂ hybrid formation were achieved by tectomer phase transfer from aqueous solution. CPO and H₂O form a two-phase system, where CPO is located in the upper layer due to its lower density. Thus, a 2 mg ml⁻¹ oligoglycine aqueous solution was added 1:1 to a MoS₂ dispersion in CPO. The two-phase system consisting of MoS₂-containing CPO (upper phase) and tectomer solutions (lower phase) was vigorously shaken by hand and then let settle for 24 h. Tectomer/MoS₂ hybrids were collected from the CPO upper phase and characterised by XPS.

A similar procedure was followed for graphene (from Aldrich ref#900561). Thus, a dispersion of graphene in CPO (2 mg ml⁻¹) was prepared by sonication and then a 2 mg ml⁻¹ oligoglycine aqueous solution was added 1:1. The two-phase system was vigorously shaken by hand and then left for 24 h. Tectomer/graphene hybrids collected from the aqueous lower phase were characterised by XPS.

4.4. AFM measurements

AFM characterisation is performed by Bruker Dimension Icon with PF-QNM (PeakForce-Quantitative NanoMechanical) mode. Tectomer functionalised probe is made by dipping SCM-PIT tip into tectomer solution for 30 min. Multiple dip coatings have been performed to ensure complete coating of the probe. Adhesion is measured by the pull-out force in the force–distance curve when the tip leaves the surface. This force corresponds to the interaction between tectomer and the measured sample.

4.5. Raman spectroscopy

Raman spectroscopy is carried out by Renishaw inVia™ confocal Raman microscope with 0.8 cm⁻¹ spectral resolution and 532 nm laser (type: solid state, model: RL53250). The 1800 mm⁻¹ grating in 100× magnification and 5 mW laser power is used. The peak position and peak intensity are then evaluated by Lorentz fitting.

4.6. Electron microscopy characterisation

TEM, Tecnai F30, FEI microscopes were used to characterise the structural features of tectomers and MoS₂ platelets and their interaction in the hybrids. Samples for TEM imaging were prepared depositing a droplet of dispersions of the tested materials onto carbon-coated copper grids (previously treated in a UV–ozone chamber for 5 min). The samples were allowed to dry under ambient conditions after wicking away most of the solution.

SEM characterisation was performed with an Inspect F50 field emission SEM microscope (FEI). Samples were coated with a 14 nm thick palladium layer by sputtering prior to SEM imaging. Energy dispersive x-ray spectroscopy allowed us to allocate MoS₂ nanosheets in tectomer/MoS₂ hybrids.

4.7. X-ray photoelectron spectroscopy (XPS)

XPS was performed on drop-cast dispersions dried at room temperature on Al foil using an ESCA Plus Omicron spectrometer provided with a Mg anode (1253.6 eV) working at 225 W (15 mA, 15 kV). BE positions were corrected by setting sp³ carbon at a BE = 284.8 eV. CASA software was used for the peak deconvolution and Shirley type baseline correction was applied.

4.8. Graphene and MoS₂ chemiresistor

The microscale electrical response for the interaction between the 2D materials and tectomer were carried out over interdigitated electrodes (IDEs). Mechanically exfoliated few layers of graphene and MoS₂ are deposited over the IDEs gold electrodes. ME 2D materials are preferred over CVD based 2D materials due to their crystalline nature, mitigation of structural defects (such as grain boundaries in graphene), and unwanted organic residue appeared during wet transfer. Difference in the electrical response (Δ) has been measured in pre and post deposition of the tectomers through I – V curves as a function of different voltages (–2 to 2 V) and as a function of time (s) to monitor the doping effect from tectomer.

Data availability statement

All data that support the findings of this study are included within the article (and any supplementary files).


Acknowledgments

We would like to acknowledge strategic development funding from the University of Sussex. Additional funding from the Aragon Government is also acknowledged (Grupo de Nanosensores y Sistemas Bioanalíticos (N&SB), ref. E25_20R). Authors acknowledge the use of instrumentation as well as the technical advice provided by the National Facility ELECM ICTS, node ‘Laboratorio de Microscopías Avanzadas’ at University of Zaragoza. The authors thank Alfonso Ibarra and Gala Simón for valuable technical support and fruitful discussions. This work was also partially supported by a UKRI Future Leaders Fellowship (Grant No. MR/T042664/1). Dedicated to our dear friend and colleague Dr Alexander Zakhidov (1981–2021).

ORCID iDs

Manoj Tripathi  <https://orcid.org/0000-0002-8052-428X>

Rosa Garriga  <https://orcid.org/0000-0003-2607-7834>

Sean P Ogilvie  <https://orcid.org/0000-0002-0433-8186>

Aline Amorim Graf  <https://orcid.org/0000-0003-3071-2255>
 Matthew J Large  <https://orcid.org/0000-0001-7295-7619>
 Peter J Lynch  <https://orcid.org/0000-0001-8805-0632>
 Konstantinos Papagelis  <https://orcid.org/0000-0001-5094-9837>
 John Parthenios  <https://orcid.org/0000-0001-6066-7120>
 Vicente L Cebolla  <https://orcid.org/0000-0002-9786-9217>
 Izabela Jurewicz  <https://orcid.org/0000-0003-0237-8384>
 Alan B Dalton  <https://orcid.org/0000-0001-8043-1377>
 Edgar Muñoz  <https://orcid.org/0000-0001-9309-2394>

References

- [1] Loan P T K, Zhang W, Lin C-T, Wei K-H, Li L-J and Chen C-H 2014 Graphene/MoS₂ heterostructures for ultrasensitive detection of DNA hybridisation *Adv. Mater.* **26** 4838–44
- [2] Dean C R *et al* 2010 Boron nitride substrates for high-quality graphene electronics *Nat. Nanotechnol.* **5** 722–6
- [3] Yu L *et al* 2014 Graphene/MoS₂ hybrid technology for large-scale two-dimensional electronics *Nano Lett.* **14** 3055–63
- [4] Liu X and Li Z 2015 Electric field and strain effect on graphene-MoS₂ hybrid structure: *ab initio* calculations *J. Phys. Chem. Lett.* **6** 3269–75
- [5] Roy K, Padmanabhan M, Goswami S, Sai T P, Ramalingam G, Raghavan S and Ghosh A 2013 Graphene-MoS₂ hybrid structures for multifunctional photoresponsive memory devices *Nat. Nanotechnol.* **8** 826–30
- [6] Xu H, Wu J, Feng Q, Mao N, Wang C and Zhang J 2014 High responsivity and gate tunable graphene-MoS₂ hybrid phototransistor *Small* **10** 2300–6
- [7] Sachs B, Britnell L, Wehling T O, Eckmann A, Jalil R, Belle B D, Lichtenstein A I, Katsnelson M I and Novoselov K S 2013 Doping mechanisms in graphene-MoS₂ hybrids *Appl. Phys. Lett.* **103** 251607
- [8] Choi M S, Lee G-H, Yu Y-J, Lee D-Y, Lee S H, Kim P, Hone J and Yoo W J 2013 Controlled charge trapping by molybdenum disulphide and graphene in ultrathin heterostructured memory devices *Nat. Commun.* **4** 1624
- [9] McGilly L J *et al* 2020 Visualization of moiré superlattices *Nat. Nanotechnol.* **15** 580–4
- [10] Mao X-R, Shao Z-K, Luan H-Y, Wang S-L and Ma R-M 2021 Magic-angle lasers in nanostructured moiré superlattice *Nat. Nanotechnol.* **16** 1099–105
- [11] Sun X, Fan J, Fu C, Yao L, Zhao S, Wang J and Xiao J 2017 WS₂ and MoS₂ biosensing platforms using peptides as probe biomolecules *Sci. Rep.* **7** 10290
- [12] Li C, Adamcik J and Mezzenga R 2012 Biodegradable nanocomposites of amyloid fibrils and graphene with shape-memory and enzyme-sensing properties *Nat. Nanotechnol.* **7** 421–7
- [13] Walsh T R and Knecht M R 2019 Biomolecular material recognition in two dimensions: peptide binding to graphene, h-BN, and MoS₂ nanosheets as unique bioconjugates *Bioconjug. Chem.* **30** 2727–50
- [14] Zuo X, Dai H, Zhang H, Liu J, Ma S and Chen X 2018 A peptide-WS₂ nanosheet based biosensing platform for determination of β -secretase and screening of its inhibitors *Analyst* **143** 4585–91
- [15] Wang L, Zhang Y, Wu A and Wei G 2017 Designed graphene-peptide nanocomposites for biosensor applications: a review *Anal. Chim. Acta* **985** 24–40
- [16] Qian Y, Di S, Wang L and Li Z 2021 Recent advances in the synthesis and applications of graphene-polypeptide nanocomposites *J. Mater. Chem. B* **9** 6521–35
- [17] Russell S R and Claridge S A 2016 Peptide interfaces with graphene: an emerging intersection of analytical chemistry, theory, and materials *Anal. Bioanal. Chem.* **408** 2649–58
- [18] Georgakilas V, Otyepka M, Bourlino A B, Chandra V, Kim N, Kemp K C, Hobza P, Zboril R and Kim K S 2012 Functionalization of graphene: covalent and non-covalent approaches, derivatives and applications *Chem. Rev.* **112** 6156–214
- [19] Zhang P, Wang Z, Liu L, Klausen L H, Wang Y, Mi J and Dong M 2019 Modulation the electronic property of 2D monolayer MoS₂ by amino acid *Appl. Mater. Today* **14** 151–8
- [20] Moses P G, Mortensen J J, Lundqvist B I and Nørskov J K 2009 Density functional study of the adsorption and van der Waals binding of aromatic and conjugated compounds on the basal plane of MoS₂ *J. Chem. Phys.* **130** 104709
- [21] Wang X, Gao D, Li M, Li H, Li C, Wu X and Yang B 2017 CVD graphene as an electrochemical sensing platform for simultaneous detection of biomolecules *Sci. Rep.* **7** 1–9
- [22] Farimani A, Min K and Aluru N 2014 DNA base detection using a single-layer MoS₂ *ACS Nano* **8** 7914–22
- [23] Zhang L, Lu Z, Song Y, Zhao L, Bhatia B, Bagnall K R and Wang E N 2019 Thermal expansion coefficient of monolayer molybdenum disulfide using micro-Raman spectroscopy *Nano Lett.* **19** 4745–51
- [24] Yoon J, Lee S N, Shin M K, Kim H-W, Choi H K, Lee T and Choi J-W 2019 Flexible electrochemical glucose biosensor based on GOx/gold/MoS₂/gold nanofilm on the polymer electrode *Biosens. Bioelectron.* **140** 111343
- [25] Xu S, Feng X, Gao T, Liu G, Mao Y, Lin J, Yu X and Luo X 2017 Aptamer induced multicoloured Au NCs-MoS₂ 'switch on' fluorescence resonance energy transfer biosensor for dual color simultaneous detection of multiple tumor markers by single wavelength excitation *Anal. Chim. Acta* **983** 173–80
- [26] Lee J E, Ahn G, Shim J, Lee Y S and Ryu S 2012 Optical separation of mechanical strain from charge doping in graphene *Nat. Commun.* **3** 1–8
- [27] Michail A, Delikoukos N, Parthenios J, Galotis C and Papagelis K 2016 Optical detection of strain and doping inhomogeneities in single layer MoS₂ *Appl. Phys. Lett.* **108** 173102
- [28] Ferralis N 2010 Probing mechanical properties of graphene with Raman spectroscopy *J. Mater. Sci.* **45** 5135–49
- [29] Lazzeri M and Mauri F 2006 Nonadiabatic Kohn anomaly in a doped graphene monolayer *Phys. Rev. Lett.* **97** 266407
- [30] Chakraborty B, Bera A, Muthu D V S, Bhowmick S, Waghmare U V and Sood A K 2012 Symmetry-dependent phonon renormalization in monolayer MoS₂ transistor *Phys. Rev. B* **85** 161403
- [31] Oliveira M, Chasqueira F, Arantes-Oliveira S and Pessanha S 2018 The use of micro-Raman spectroscopy for the analysis of caries-affected dentin adhesive interfaces *Int. J. Adhes. Adhes.* **87** 216–22
- [32] Elinski M B, Menard B D, Liu Z and Batteas J D 2017 Adhesion and friction at graphene/self-assembled monolayer interfaces investigated by atomic force microscopy *J. Phys. Chem. C* **121** 5635–41
- [33] Li B, Yin J, Liu X, Wu H, Li J, Li X and Guo W 2019 Probing van der Waals interactions at two-dimensional heterointerfaces *Nat. Nanotechnol.* **14** 567–72
- [34] Garriga R, Jurewicz I, Romero E, Jarne C, Cebolla V L, Dalton A B and Muñoz E 2016 Two-dimensional, pH-responsive oligoglycine-based nanocarriers *ACS Appl. Mater. Interfaces* **8** 1913–21
- [35] Garriga R *et al* 2017 Multifunctional, biocompatible and pH-responsive carbon nanotube-and graphene

- oxide/tectomer hybrid composites and coatings *Nanoscale* **9** 7791–804
- [36] Garriga R, Jurewicz I, Seyedin S, Tripathi M, Pearson J R, Cebolla V L, Dalton A B, Razal J M and Muñoz E 2019 Two-dimensional oligoglycine tectomer adhesives for graphene oxide fiber functionalization *Carbon* **147** 460–75
- [37] Jurewicz I *et al* 2018 Functionalization of silver nanowire transparent electrodes with self-assembled 2-dimensional tectomer nanosheets *ACS Appl. Nano Mater.* **1** 3903–12
- [38] Pimenta M A, del Corro E, Carvalho B R, Fantini C and Malard L M 2015 Comparative study of Raman spectroscopy in graphene and MoS₂-type transition metal dichalcogenides *Acc. Chem. Res.* **48** 41–47
- [39] Li H, Zhang Q, Yap C C R, Tay B K, Edwin T H T, Olivier A and Baillargeat D 2012 From bulk to monolayer MoS₂: evolution of Raman scattering *Adv. Funct. Mater.* **22** 1385–90
- [40] Rice C, Young R J, Zan R, Bangert U, Wolverson D, Georgiou T, Jalil R and Novoselov K S 2013 Raman-scattering measurements and first-principles calculations of strain-induced phonon shifts in monolayer MoS₂ *Phys. Rev. B* **87** 081307
- [41] Tsygankova S V, Chinarev A A, Tuzikov A B, Severin N, Kalachev A A, Rabe J P, Gambaryan A S and Bovin N V 2014 Biantennary oligoglycines and glyco-oligoglycines self-associating in aqueous medium *Beilstein J. Org. Chem.* **10** 1372–82
- [42] Jiang T, Wang Z, Ruan X and Zhu Y 2018 Equi-biaxial compressive strain in graphene: Grüneisen parameter and buckling ridges *2D Mater.* **6** 015026
- [43] Mescola A *et al* 2021 Graphene confers ultralow friction on nanogear cogs *Small* **17** 2104487
- [44] Pierucci D *et al* 2016 Large area molybdenum disulphide-epitaxial graphene vertical van der Waals heterostructures *Sci. Rep.* **6** 26656
- [45] Das A *et al* 2008 Monitoring dopants by Raman scattering in an electrochemically top-gated graphene transistor *Nat. Nanotechnol.* **3** 210–5
- [46] Brown N M D, Cui N and McKinley A 1998 An XPS study of the surface modification of natural MoS₂ following treatment in an RF-oxygen plasma *Appl. Surf. Sci.* **134** 11–21
- [47] Azcatl A *et al* 2016 Covalent nitrogen doping and compressive strain in MoS₂ by remote N₂ plasma exposure *Nano Lett.* **16** 5437–43
- [48] McDonnell S, Addou R, Buie C, Wallace R M and Hinkle C L 2014 Defect-dominated doping and contact resistance in MoS₂ *ACS Nano* **8** 2880–8
- [49] Tripathi M, Mahmood H, Novel D, Iacob E, Vanzetti L, Bartali R, Speranza G, Pegoretti A and Pugno N 2018 Nanoscale friction of graphene oxide over glass-fibre and polystyrene *Composites B* **148** 272–80
- [50] Lee N J, Yoo J W, Choi Y J, Kang C J, Jeon D Y, Kim D C, Seo S and Chung H J 2009 The interlayer screening effect of graphene sheets investigated by Kelvin probe force microscopy *Appl. Phys. Lett.* **95** 222107
- [51] Kim J H, Lee J, Kim J H, Hwang C C, Lee C and Park J Y 2015 Work function variation of MoS₂ atomic layers grown with chemical vapor deposition: the effects of thickness and the adsorption of water/oxygen molecules *Appl. Phys. Lett.* **106** 251606
- [52] Tripathi M *et al* 2021 Structural defects modulate electronic and nanomechanical properties of 2D materials *ACS Nano* **15** 2520–31
- [53] Dolui K, Rungger I and Sanvito S 2013 Origin of the n-type and p-type conductivity of MoS₂ monolayers on a SiO₂ substrate *Phys. Rev. B* **87** 165402
- [54] Michail A, Parthenios J, Anastopoulos D, Galiotis C, Christian M, Ortolani L, Morandi V and Papagelis K 2018 Controllable, eco-friendly, synthesis of highly crystalline 2D-MoS₂ and clarification of the role of growth-induced strain *2D Mater.* **5** 035035